Experiments on exotic atom spectroscopy

D. Gotta

Institut für Kernphysik, Forschungszentrum Jülich, D-52425 Jülich, Germany

Abstract Results are reviewed from recent exotic atom experiments using a focussing Bragg spectrometer. The measured energies of the Lα X-rays from antiprotonic hydrogen and deuterium and the Kα transition from pionic deuterium are compared to the transition energies as calculated from quantum electrodynamics in order to determine the strong interaction antiproton-nucleon and pion-nucleon scattering parameters at threshold. A high precision experiment to determine the mass of the charged pion to 1ppm has been started by investigating the transitions in pionic nitrogen, where the occurance of Coulomb explosion has been seen now directly from the Doppler broadening. In a forthcoming high precision experiment of the pion-nucleon scattering length new calibration methods using an ECR source will be used to connect energy standards both from exotic and electronic atoms. Such techniques offer the possibility of high precision studies in few electron systems.

1 Introduction

Atoms in which the electron shell is replaced partly or in total by other elementary particles of negative charge are called exotic atoms. Up to now, the systems with muons, pions, kaons, antiprotons, and sigma hyperons have been established. Muonic and pionic atoms are being investigated since years at the meson factories of the Paul-Scherrer-Institut (PSI), TRIUMF, or earlier at LAMPF. At CERN in the years 1983 until 1996, the Low-Energy-Antiproton-Ring (LEAR) provided high-quality low-energy antiproton beams, which were especially suited for stop experiments and thus for the formation of antiprotonic atoms.

Normally, the observables in the X-ray spectroscopy of exotic atoms are the energies and the intensities of the radiation, which is emitted during the deexcitation of the atomic system. From the line intensities, conclusions are drawn both for the capture process and the interaction with the remaining part of the electron cloud and processes originating from the interaction with neighbouring target atoms during the first steps of the atomic cascade. In the lower part of the cascade, the exotic atom can be prepared as a hydrogen-like system when suitable experimental conditions are chosen. Such hydrogen-like atoms may then serve as a testing ground for the calculations of transition energies and to investigate the properties of the captured particle itself. At smaller distances, i.e. for the low-lying states, the influence of the finite nuclear size on the binding energy increases and, for strongly interacting particles, the effects of the nuclear forces become more and more visible. Of special interest are the elementary systems formed with the hydrogen isotopes to study the strong pion- and antiproton-nucleon interaction at threshold. Thus, the X-ray spectroscopy of exotic atoms offers access to a large variety of problems [1–5].

The precise calculation of the binding energies has to use the relativistic description as given by the Dirac or the Klein-Gordon formula and, in addition, has to include the contributions of quantum electrodynamics (QED), relativistic recoil corrections, and polarisation effects. Due to the large mass of the 'orbiting' particle, the predominant QED contribution in exotic atoms is vacuum polarisation, in contrast to self energy as in the case of electronic atoms [2,6,7]).

Highest energy resolution for X-rays in the few keV range is achievable only with crystal spectrometers which, however, on principle are devices of low efficiency. Although high fluxes are reached in the beam lines of the meson factories, the experimental challenge is to achieve a high resolution together with sufficient count rates as well as to achieve stable conditions for the nevertheless unavoidable long measuring periods. It is essential to use the particle flux provided by the accelerator in an optimal way and to maximize both the line yields of the X-ray transitions and the detection efficieny up to the theoretical limits.

In particular for the atoms formed with the hydrogen isotopes, high line yields can be obtained only with gas targets. A crystal spectrometer, however, requires a small and bright X-ray source which cannot be achieved with the usual linear set-up to stop the beam. Sufficient stop densities are available if for degrading and stopping of the beam the cyclotron trap is used. For such experiments with low counting rates an efficient background suppression is essential. It is achieved by the use of Charge-Coupled-Devices (CCDs) as X-ray detectors (Figure 1).

2 Formation and atomic cascade of exotic atoms

After slowing down to a kinetic energy of a few eV, negatively charged particles are captured in the Coulomb field of atoms into highly excited atomic levels by the emission of electrons. The depletion of the electron cloud proceeds shell by shell by continued emission of Auger electrons as soon as the energy difference between two exotic atom levels exceeds the ionisation energy. Thus, the lighter exotic atoms in the end become hydrogen-like systems provided no electron refilling occurs as is the case for dense or solid targets [8,9]. In the lower part of the atomic cascade, the deexcitation by emission of X-ray quanta dominates even in the presence of electrons.

The dimensions of exotic atoms are obtained by replacing the electron's mass in the expression for the Rydberg energy by the reduced mass m_{red} of the particle-nucleus system. During the last steps of the atomic cascade the extensions of exotic atoms are already closer to nuclear dimensions than to the atomic scale. There, in the case of hadrons the electromagnetic deexcitation then has to compete with channels opened by the strong interaction. A detailed discussion of the atomic cascade may be found in [4,10,11].

Exotic hydrogen occupies a special position regarding the interaction with the target material. It is electrically neutral and, therefore, can easily penetrate the Coulomb field of neighbouring atoms. This leads to a drastic reduction of the X-ray yields in pionic and antiprotonic hydrogen (Day-Snow-Sucher-effect [12]), because in the high angular momentum states now s- and p-wave contributions are induced and in hadronic atoms an admixture of s- or p-waves leads with high probability to annihilation. For atomic levels with large n the Stark mixing prevails all other internal and external deexcitation processes. Hence, for hydrogen the use of low pressure gas targets is indispensible to achieve high X-ray yields [13].

3 Experiment

3.1 Cyclotron trap and X-ray source

A focussing Bragg crystal spectrometer requires a small and bright X-ray source having an extension matched as good as possible to the extension of the line pattern to be observed. Such conditions are achieved when the cyclotron trap is used, a device which was designed to obtain high stop densities with muon, pion, and antiproton beams [8,9,14–17]. The range curve of the beam is wound up in a magnetic field with focussing properties which is produced by two superconducting coils. Between the coils, the target chamber is installed containing a suitable degrader arrangement and the target gas. The particles loose kinetic energy first in the degraders and

in the target gas itself thus approaching the center of the magnet on spiral orbits, and finally are stopped in a volume of a few cm^3 even at low gas pressures.

3.2 Crystal spectrometer

For X-radiation with energies below 20 keV, because of the absorption losses, reflection type crystal spectrometers are used. The X-rays are scattered at the electrons of atoms arranged regularly in lattice planes having the distance d. According to Bragg's law, $n\lambda = 2d \cdot \sin\Theta_B$, a coherent superposition for one wave length λ occurs only at the Bragg angles Θ_B, where n is the order of reflection. The width of the angular distribution of a parallel beam (rocking curve width) reflected from a plane crystal yields consequently the theoretical limit for the energy resolution. It is given only by the intrinsic properties of the material and the wave length. Usually quartz or silicon crystals are used, which behave like ideal crystals. The intrinsic properties can be calculated from the dynamical theory to one per cent or better except in the close vicinity of absorption edges [18–21].

For the investigation of broad X-ray lines or multiplets, horizontally bent crystals are of great advantage (Johann geometry), because here an energy interval according to the width of the source can be recorded simultaneously with two-dimensional position-sensitive detectors [22]. Thus, an acceptable duration of measuring periods of a few days per transition becomes possible. To achieve in addition partial vertical focussing, spherically bent crystals were used [23]. The reduced height of the image then allows the efficient use of the rather small pixel detectors like CCDs.

An accuracy of up to 10^{-6} is aimed at for the energy measurement in the described experiments, which requires an energy resolution of the order of 10^{-4}. Such values are reached in the few keV range with quartz and silicon crystals having bending radii of about 3 m and Bragg angles larger than 45 degrees, where the geometrical abberation accounts at maximum to 10^{-4} and, hence, does not abolish the intrinsic resolution of the crystal lattice. The overall efficiency of such a spectrometer is about 10^{-6} for crystal areas of 75 cm^2.

CCDs are the optimal detectors for recording X-rays in a high background environment because of their distinguished two-dimensional position resolution together with an excellent energy resolution ($\Delta E = 150$ eV at 6 keV) [24–26]. Because the charge produced by one X-ray is deposited in one or two pixels only and particle- or Compton-induced events produce larger clusters, the pixel structure allows by analysing the hit pattern an almost complete separation of X-ray and background events. Thus, for the long measuring periods, an efficient background suppression is obtained.

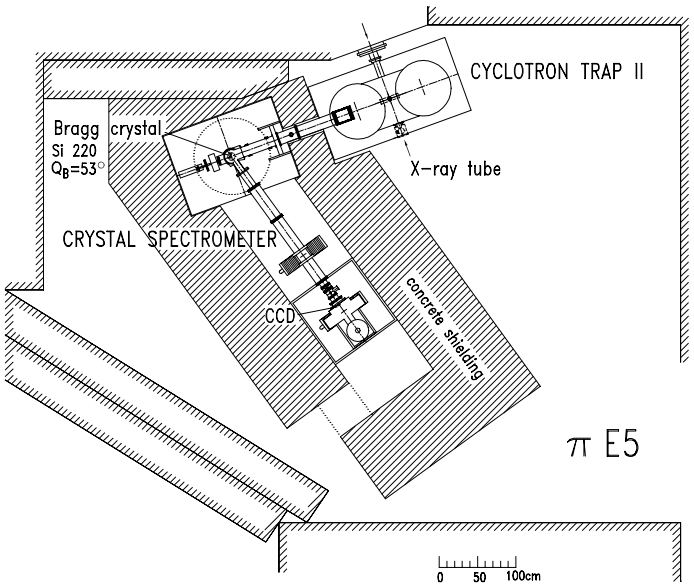

Figure 1: Set-up of cyclotron trap, crystal spectrometer and CCD detector for the pion mass experiment at PSI (from [26,27]). The massive concrete shielding is essential to suppress the neutron-induced background.

3.3 Absolute calibration

The precision envisaged requires an energy calibration and a determination of the spectrometer resolution function at a high level. In practise, both fluorescence X-rays (Table 1) and exotic X-ray transitions (Tables 2 and 4) must be used up to now. Narrow nuclear γ-rays with sufficient yields are not available in the few keV range for practical cases.

Fluorescence X-rays excited by means of an X-ray tube are always at disposal. The precise adjustment of the Bragg angle and the accumulation of spectra with high statistics can be performed within a short time and tests of stability are possible without significant losses of beam time. From those elements, where the line shapes have been determined precisely, energy calibrations can be obtained. The large natural line width, however, does not allow the determination of the resolution of the spectrometer with sufficient accuracy. An even more severe problem is to associate with the position of a fluorescence line a wave length because of the presence of satellite transitions originating from multiple ionisation.

Though beam time consuming, transitions of completely ionised exotic atoms are ideal calibration lines. The atomic levels must not be affected by the strong interaction or the presence of remaining electrons in order to make use of the precise results from the QED calculations. The natural line

Table 1: Energies E_X and natural line widths Γ_X of Kα fluorescence X-rays (in eV).

	Kα_2		Kα_1	
	E_X	Γ_X	E_X	Γ_X
Si	1739.39 ± 0.03	0.539 ± 0.070	1739.986 ± 0.019	0.524 ± 0.035
S	2306.70 ± 0.04	0.722 ± 0.047	2307.89 ± 0.030	0.769 ± 0.026
Cl	2620.85 ± 0.04	0.945 ± 0.063	2622.44 ± 0.040	0.925 ± 0.086
Sc			4090.6 ± 0.1	1.05
Cu			8047.838 ± 0.006	2.26 ± 0.02

Si, S, and Cl: [28]; Sc: [29,30]; Cu: [31]

widths are of the order of a few meV only and, therefore, can be neglected compared to the typical resolution of a few 100 meV of the spectrometer. The resolution functions are obtained from such narrow transitions having energies as close as possible to the measured transitions. Unfortunately, not in all cases a calibration line from an exotic atom with an energy close enough is available to serve also as an energy calibration.

The absolute energy is determined from the Bragg angle difference to an X-ray line of known energy. The angle difference according to the rotation of the crystals is measured with a precision absolute angular encoder having an accuracy of ± 0.2 seconds of arc (or 1ppm) for small angle differences. The total difference of the Bragg angle for two lines is given by the values obtained from the angular encoder and the positions of transitions as measured at the CCD detectors. In general, some (small) corrections for the index of refraction, the bending, and the penetration depth in the crystal have to be applied in order to obtain the final value for the Bragg angle and from that for the transition energy (see also [26]).

4 Antiprotonic hydrogen and deuterium

The hadronic part of the antinucleon-nucleus potential causes an energy shift ϵ of the atomic levels as determined by the pure Coulomb interaction. Furthermore, the occurance of annihilation reduces the life time of low-lying atomic states leading to an additional level broadening Γ. Shift and broadening are related to the complex scattering lengths of the nucleus-particle system [32–38]. The spectroscopy of hadronic atoms, therefore, is equivalent to a scattering experiment directly at threshold. The strong interaction shift and broadening of the 2p levels in antiprotonic hydrogen and deuterium was directly measured by LEAR experiment PS207 [39].

4.1 Electromagnetic level energies and hyperfine structure

The mean Lα transition energy without the influence of the strong interaction has been calculated by Barmo, Pilkuhn, and Schlaile [40], Borie [7], and recently by Boucard and Indelicato [41] yielding slightly different values (Table 2). For the hyperfine splittings, however, the results deviate significantly (Table 3). The origin of these discrepancies is supposed to stem from the treatment of the (g-2) corrections [42].

Table 2: Calculated electromagnetic transition energies of the antiprotonic lines (in eV). The values correspond to the center of gravity of the corresponding fine or hyperfine structure multiplets.

$\bar{p}\,^3$He(5g-4f)	$\bar{p}$H(3d-2p)	$\bar{p}$D(3d-2p)	$\bar{p}\,^{20}$Ne(13o-12n)	ref.
1686.49	1736.80	2316.47		[40]
1686.50	1736.81	2316.50	2444.10	[7]
1686.477	1736.798	2316.483	2444.035	[41]

In light antiprotonic atoms, the masses of the 'nucleus' and the 'orbiting' particle are (almost) equal and, therefore, also are the magnetic moments. Hence, for the hydrogen isotopes both the fine and the hyperfine structure splitting is of the order $\Delta E_{FS} \approx \Delta E_{HFS} \approx \alpha^2 \cdot B_1$. Owing to the large mass, the recoil corrections due to the anomalous magnetic moment of the proton and antiproton are significant. Therefore, for example the level ordering in protonium is no longer the same as in the analogue system positronium [40,41,43].

Because of the complex multiplet structure, the extraction of hadronic parameters demands the precise knowledge of the electromagnetic hyperfine splitting. The Lα line consists altogether of 11 transitions in the case of hydrogen and of 21 transitions for deuterium. Because of the rather small splitting of the 3d levels as compared to the 2p levels, the line shape of the 3d-2p transition yields already the 2p level structure in good approximation.

4.2 Nuclear polarisation

The electric force induces a dipole in the extended charge distributions both in the orbiting particle and in the nucleus. In light atoms, the energy shifts of the 2p and higher levels caused by the polarisation of pions and antiprotons usually are 1 meV or less and, hence, far below the experimental accuracy. Only for deuterium, due to its large quadrupole moment, the polarisation shift ΔE_{pol} in the 2p level reaches already sizeable values. Following the approach of [45] and using $\alpha_{pol}(D) = 0.633\,\mathrm{fm}^3$ for the polar-

Table 3: Predictions for the electromagnetic hyperfine splittings of the 2p und 3d levels (notation: $n^{2S+1}L_F$) in hydrogen and deuterium (in meV). The spin factor w = (2F+1)/Σ(2F+1) corresponds to a statistical population of the sublevels. A positive sign of the electromagnetic shift ΔB_{QED} stands for a more strongly bound atomic level.

HFS	w	ΔB_{QED}	ΔB_{QED}	HFS	w	ΔB_{QED}	ΔB_{QED}
$\bar{p}$H							
$2\ ^3P_2$	5/12	- 60	- 13	$3\ ^3D_3$	7/20	- 7	- 2
$2\ ^3P_1$	3/12	+ 16	+ 51	$3\ ^3D_2$	5/20	+ 1	+ 6
$2\ ^1P_1$	3/12	0	- 97	$3\ ^1D_2$	5/20	0	- 9
$2\ ^3P_0$	1/12	+ 249	+ 203	$3\ ^3D_1$	3/20	+ 16	+ 9
		[44]	[41]			[44]	[41]
$\bar{p}$D							
$2\ ^4P_{5/2}$	6/18	+ 104	- 8	$3\ ^4D_{7/2}$	8/30	+ 12	- 1
$2\ ^4P_{3/2}$	4/18	- 362	- 103	$3\ ^2D_{5/2}$	6/30	+ 29	- 4
$2\ ^2P_{3/2}$	4/18	+ 194	+ 33	$3\ ^4D_{5/2}$	6/30	- 38	+ 9
$2\ ^4P_{1/2}$	2/18	- 353	- 28	$3\ ^2D_{3/2}$	4/30	+ 3	- 6
$2\ ^2P_{1/2}$	2/18	+ 376	+ 40	$3\ ^4D_{3/2}$	4/30	- 11	+ 2
				$3\ ^4D_{1/2}$	2/30	- 6	- 2
		[40]	[41]			[40]	[41]

isibility of the deuterons [46], a change of ΔE_{pol} = - 6.6 meV is calculated for the 3d-2p transition energy.

4.3 Interaction with the external magnetic field

The static magnetic interaction energy $\mu_N \cdot B_{cyc}$ of a nuclear magneton in the external field of the cyclotron trap (of about 3 T) amounts to 90 neV, which is 1ppm of the 2p - hyperfine splitting. Also, the movement of the antiprotonic atom induces only a negligibly small electric field $\vec{E} = \vec{v} \times \vec{B}_{cyc}$ ('motional' Stark effect) when compared to the strength of the internal field. Assuming a velocity of $v = 10^6$ cm/s, corresponding to a kinetic energy of 1 eV for the antiprotonic atom [14], an electric field strength of $E \approx 3 \cdot 10^6$ V/m results. The strength of the internal Coulomb field, however, reaches values of 10^{11} V/m already at radii corresponding to n = 40.

4.4 Results for the 2p multiplet in antiprotonic hydrogen

The measurement of the hadronic parameters of the 2p state tests explicitely the long range part of the antinucleon-nucleon interaction [34]. Using the Lα transition, antiprotonic hydrogen offers the unique possibility to prepare

the antiproton-proton system in a pure p-wave state. Almost 99% of the antiprotons reaching the 2p level annihilate there, as seen from the large spin-averaged 2p level broadening of (34.0±2.9) meV, which has been determined earlier from the intensity balance of the total Balmer series to the Lyman α transition [14]. In gaseous targets, annihilation at rest occurs mainly from the atomic p states because of the reduced Stark mixing [13]. The fraction of absorption from the 3d level is predicted to be 1% only [34]. This is in agreement with the nonobservation of hadronic effects, which should show up in the line yields of the Balmer series for hydrogen or deuterium [14]. Therefore, the 2p hyperfine levels are assumed to be populated according to their statistical weight.

The line profile of the 3d-2p transition in antiprotonic hydrogen exhibits a shoulder at the high energy side (Figure 2). It is interpreted as the 2^3P_0 hyperfine state, because its relative intensity - obtained to (7.9±1.0)% in a free fit to the line profile - is in good agreement with the statistical population of 8.3% for the 2^3P_0 level (Table 3). The main part of the line consists of the 3 - not resolved - components $2(^3P_2,^3P_1,^1P_1)$.

The 2^3P_0 state plays a particular role. Its shift and broadening is predicted to about 100 meV which is verified by the experiment yielding (120±25) meV [47] when the result from the recent QED calculation is used [41]. Such large hadronic effects in the 2^3P_0 state are mandatory for the meson-exchange model from which the real part of the antinucleon-nucleon potential is derived [34,48,49]. The value obtained for the spin-averaged shift of the group $2(^3P_2,^3P_1,^1P_1)$ is compatible with zero and the spin-averaged broadening is of the order of the spin-averaged width as predicted [34,47]. Obviously, the level structure originating from the real part of the hadronic potential is not destroyed by the very fast annihilation. The experimental results are considered as strong support for the validity of the meson-exchange models to describe the long-range real part of the low-energy antinucleon-nucleon interaction.

4.5 Results for the 2p multiplet in antiprotonic deuterium

In antiprotonic deuterium, at present the only possibility to determine any hadronic effects is a direct measurement of the the 2p-level width and broadening. Because of the more frequent annihilation from p levels as compared to antiprotonic hydrogen, the observation of the transitions to the atomic ground state remains doubtful because of the smaller line yields of the Lyman series and the increased hadronic broadening of the 1s level [14,50].

The two results for the QED hyperfine splitting differ considerably (Table 3). Barmo et al. predict, that the hyperfine splitting in the 2p level is dominated by the electromagnetic interaction [40]. Therefore, the 3d-2p

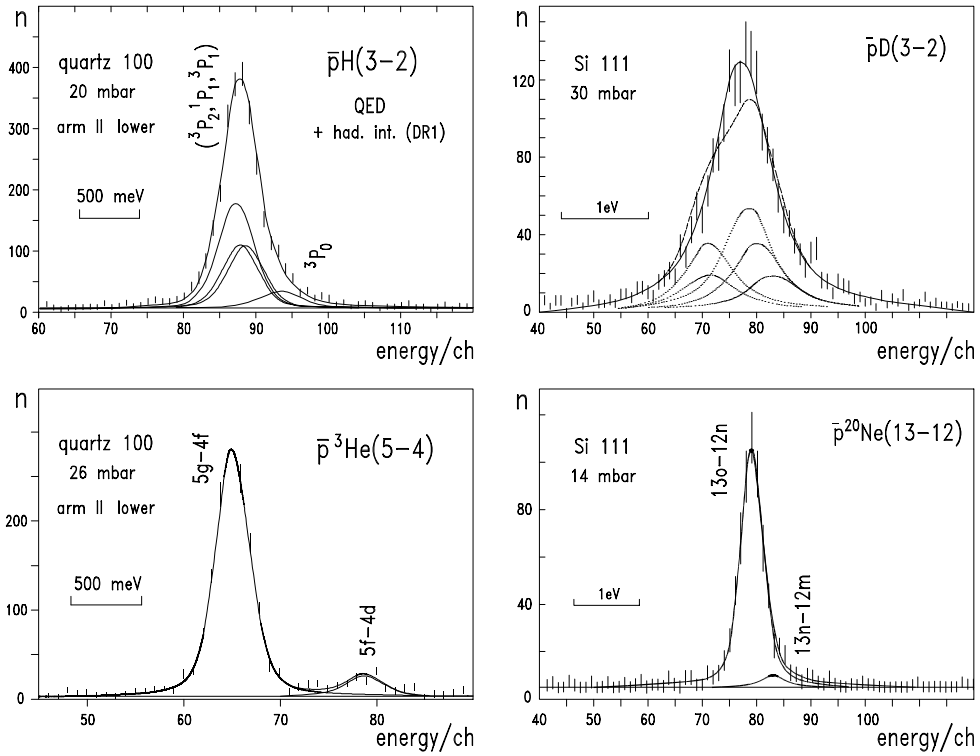

Figure 2: Line shapes of the Lα transitions in antiprotonic hydrogen and deuterium and corresponding antiprotonic calibration transitions [51].

line shape should form approximately a doublet structure from the groups $2(^4P_{3/2},^4P_{1/2},^4P_{1/2})$ and $2(^4P_{5/2},^2P_{3/2})$ showing a small tail to the high energy side stemming from the $2^2P_{1/2}$ state.

The measured line shape does not show any evidence for such a doublet structure (Figure 2). The calculation of Boucard and Indelicato yields a much smaller hyperfine splitting [41], which allows to treat the whole multiplet as a single line only in comparison with the experimental resolution. The numerical results from the single line fit are indistinguishable within the experimental errors from the results from a fit forcing the hyperfine pattern as given by Boucard and Indelicato. With that, for the spin-averaged hadronic shift and broadening $\epsilon_{2p} = (-250 \pm 26)$ meV and $\Gamma_{2p} = (489 \pm 30)$ meV is obtained [51]. The annihilation width is found about 20% smaller than in the previous analysis [52]. The shift is negative, i.e., the interaction is repulsive as predicted. For the spin-averaged broadening, the multiple scattering ansatz of Wycech, Green and Niskanen yields about 400 meV in good agreement with the experimental result, whereas the magnitude of the shift is underestimated by a factor of 5 [53].

5 Mass of the charged pion

The motivation for an improved pion mass measurement reaching an accuracy of at least 1ppm arises from several aspects. Future muon neutrino mass measurements should be able to improve their sensitivity from $170\,\mathrm{keV/c^2}$ to below $70\,\mathrm{keV/c^2}$. Theoretical considerations using the Standard Model as well as all 'popular' classes of theories which go beyond the Standard Model and take into account cosmological bounds reduce considerably the range of possible mass values. It was shown e.g. that the mass of the muon neutrino is either $\geq 70\,\mathrm{keV/c^2}$ for unstable neutrinos or $\leq 65\,\mathrm{eV/c^2}$ for stable neutrinos contributing to the matter density of the universe within the cosmological bound [54,55].

The recent highly sensitive search for Muonium - Antimuonium ($M\bar{M}$) conversion [56] aiming at an improvement in sensitivity by an order of magnitude to about 10^{-3} for $\mathrm{G}_{M\bar{M}}/\mathrm{G}_F$ would, together with a factor of almost two for a reduced upper limit of the muon neutrino mass, exclude a certain type of theories extending the Standard Model [57].

The experimental accuracy for the hadronic 1s level shift in pionic hydrogen obtained in an earlier crystal spectrometer measurement was 13 meV for the statistical and 31 meV for the systematical error [58]. The error originating from the uncertainty of the pion mass already accounts for 8 meV. The systematical error stems mainly from the limited precision of the calibration line and the lattice constant of the Bragg crystal. Such systematical errors could be reduced significantly in future independent measurements.

In order to avoid the problems inherent to energy calibrations using fluorescence X-rays or screening effects from the remaining electrons, it is proposed to obtain the absolute calibration from a muonic transition of almost equal energy as a pionic one [27]. The experiment uses the fact, that the positive muon mass is known to an accuracy of 0.32ppm and assumes CPT invariance. The requirement to measure the same transition in terms of quantum numbers and the request to use gas targets at pressures of about 1 bar led to the pair pionic nitrogen and muonic oxygen and the 5 - 4 transitions (Table 4). The natural line widths of 8 meV are negligible as compared to the experimental resolution of about 350 meV. Because of the small energy difference, the crystal spectrometer can be set up without movable parts between crystal and detector which excludes any systematic errors from the adjustment of the Bragg angle.

A feasibility study was performed with the πN(5g-4f) transition using the cyclotron trap I and the Cu Kα_1 fluorescence line as the energy calibration (Figure 3) [26]. The ambiguity of 15ppm of a previous measurement with the πMg(5g-4f) transition could be removed. There, a solid state target was used [59,60]. The ambiguity was due to the number of K electrons

Table 4: Calculated electromagnetic transition energies (in eV) of muonic and pionic X-ray lines (from [41]).

πD(2p-1s)	π^{20}Ne(7i-6h)	μ^{16}O($5g_{9/2}$-$4f_{7/2}$)	π^{14}N(5g-4f)	π^{20}Ne(6h-5g)
2597.527	2718.751	4023.757	4055.373	4509.888

present at the time of emission of the X-ray. The result of Lenz et al. [26] for the mass of the charged pion is $m_\pi = (139.57071 \pm 0.00053)\,\mathrm{MeV/c^2}$ being (+5.5±3.8)ppm larger than the result B (2 K electrons) of Jeckelmann et al. [60]. The above-mentioned value is also consistent with the limits extracted from the muon neutrino mass measurements [61].

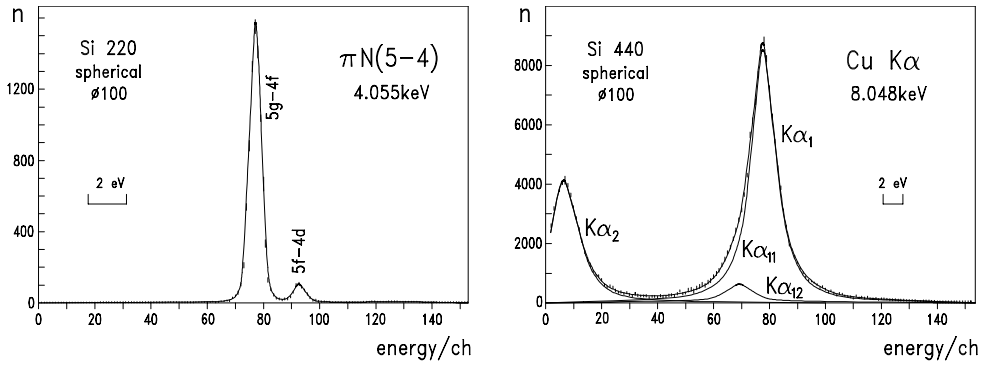

Figure 3: Measured line shapes of the πN(5g-4f) transition and the Cu Kα fluorescence line [26]. The parameters for the line shape of the Cu Kα transition have been taken from [31].

Cascade calculations based on the code of Akylas and Vogel [62] predict for nitrogen a probability of less than 2% (at a pressure of 1 bar) for one remaining K electron when the pion or muon reaches the n=5 level, which could be verified as an upper limit by the feasibility study [26].

In the forthcoming final measurement, the source of X-rays emitted by the exotic atoms will be formed by stopping the pion beam in the new cyclotron trap (ZF II). The muons originate from pion decay inside the target chamber. With the new trap a sufficently high stop density also for the decay muons has been achieved recently [63].

5.1 Test of the Klein-Gordon equation

The energy difference between the circular transition π^{14}N(5g-4f) and the next inner parallel transition π^{14}N(5f-4d) (Figure 3) was measured by Lenz

et al. to $\Delta E[(5g\text{-}4f) - (5f\text{-}4d)] = (2308.2 \pm 9.7)$ meV [26]. The precision achieved exceeds the one of earlier tests of the Klein-Gordon equation by Delker et al. [64] by a factor of about 5. A recent QED calculation of Boucard and Indelicato yielded in good agreement 2312.8 meV [41].

5.2 Direct observation of Coulomb explosion

The observed line width of about 710 meV (FWHM) of the πN (Figure 3) or the μO 5g - 4f transition is a factor 2 larger than expected from the resolution of the spectrometer [26]. First checks assumed distorted crystal material which, however, is not sufficient to explain such a broadening. On the other hand, for diatomic molecules like N_2 or O_2, a significant Doppler broadening originating from Coulomb explosion cannot be excluded. Here, the πN system gains kinetic energy, when after Auger emission of several electrons the binding of the molecular system πN_2 breaks and the two fragments of almost equal mass are accelerated by the Coulomb force. Evidence for such an effect has been deduced earlier from the different pressure dependence of the K X-ray line yields of pionic nitrogen and neon [4,65].

A measurement of the πNe(6h-5g) transition (Table 4) has been performed in order to test such a hypothesis, because the width of that reflection is only due to the experimental response function. The πNe line of 400 meV is significantly narrower than the πN and μO transitions and, therefore, the large widths of the latter are assumed to originate from Coulomb explosion [63]. The measured additional width of the pionic 5g-4f transition amounts to 400 - 575 meV depending on the details for the assumptions of the line shape of the resolution function. It corresponds to a kinetic energy of the πN system of 50 - 130 eV. Assuming that the molecule decomposes at distances comparable to the molecular bond length of 1.1×10^{-8} cm at the time of separation, for the product of the charges $q_1 \cdot q_2 \approx 9 - 20$ is obtained. Consequently, the range of charge states at the time of explosion is 3 to 4 - 5, which corresponds to the removal of 6 - 9 electrons from the N_2 molecule. Separation distances of about 5 molecular bond length as observed in the slow laser induced Coulomb explosion [66] can be excluded because a value of $q_1 \cdot q_2 = 45 - 100$ cannot be reached for nitrogen and oxygen.

6 Pionic hydrogen

The description of the pion-nucleon interaction in the confinement region is considered as a fundamental problem in QCD. The progress achieved on the theoretical side in describing low energy phenomena from basic principles in the framework of the chiral perturbation theory allows the prediction

of the pion-nucleon scattering lengths with an accuracy at the per cent level [67,68]. Consequently, the experimental information stemming from the hadronic shift and broadening of the ground state in pionic hydrogen should at least reach a precision at that level.

The last generation of experiments on pionic hydrogen and deuterium achieved already an accuracy of about 10% for the isospin separated πN scattering lengths [58,69]. Recently, new developments in the experimental techniques (see pion mass experiment) and in the atomic cascade of pionic and muonic hydrogen became available [70,71]. For a precision experiment, a detailed study of the cascade is essential in order to reach a precision of better than 2 - 3%. Below that level, Coulomb deexcitation [72], which competes with external Auger and X-ray emission during the atomic cascade, hinders the precise determination of the line width. The deexcitation energy is used to accelerate the πH system during the encounter with another atom in the target and thus, the measured line shape is composed of a superposition of many discrete Doppler profiles convoluted with the spectrometer response function. It is proposed to quantify such a complex line shape using the μH(2p-1s) transition, where the effects of Coulomb deexcitation can be studied in a system without strong interaction [73]. Inserting the knowledge from the cascade studies, an accuracy of 1% becomes feasible for the strong interaction broadening of the 1s level in pionic hydrogen.

6.1 Feasibility study with pionic deuterium

To demonstrate the count rate and background conditions for such measurements in pionic and muonic hydrogen, the 2p - 1s transition in pionic deuterium has been studied (Figure 4). The cyclotron trap II was used to stop the high intensity πE5 beam in a gas target at 2.5 bar pressure. The X-rays were measured with the focussing crystal spectrometer set-up for the pion mass measurement. As energy calibration the Kα fluorescence X-rays from chlorine have been used and the resolution function has been obtained from the narrow π^{20}Ne(7i-6h) transition.

New improved values for the strong interaction shift and broadening of the atomic ground state have been extracted from the position and line shape being $\epsilon_{1s} = -2.469 \pm 0.038 \pm 0.040$ eV and $\Gamma_{1s} = 1.09 \pm 0.129$ eV [74]. The result is in agreement with the previous measurement where the πD(3p-1s) transition and the argon Kα radiation as energy calibration was used [69]. In the calculation of the electromagnetic 2p-1s transition energy (Table 4), for the deuteron charge radius a value of 2.138 fm was used [41]. The minus sign of the shift indicates a repulsive interaction. The first error of ϵ_{1s} could be easily reduced by a high statistics measurement. The second error of ϵ_{1s} stems only from the accuracy of the energy determination of the

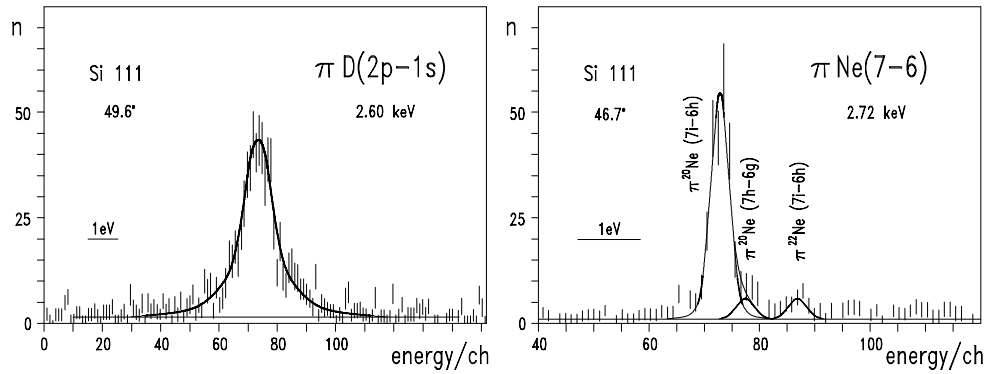

Figure 4: Left - πD(2p-1s) line shape obtained from the feasibility study for the πH experiment [73,74]. Right - reflection of the πNe(7-6) transition [63].

Kα_1 transition in chlorine (Table 1) and can only be improved when a new calibration standard will be available.

7 New calibration standards

In the few keV range, a major problem both for the energy calibration and the determination of the crystal spectrometer response function stems from the fact, that no narrow lines are available from easily accessible sources like X-ray tubes. The X-ray line widths of low Z multiple electron systems are dominated by the Auger widths and then quickly increase with the nuclear charge. The natural width usually exceeds the typical values for the spectrometer resolution by at least a factor of 3.

In addition, the line shape exhibits a complex structure due to satellite transitions originating from multiple ionisation. Although light elements like silicon and sulfur do not show pronounced satellite structures when the ionisation occurs from weakly ionising radiation like X-rays or electrons, due to the large natural widths a precise determination of the position of the diagram line (stemming from atoms with one K-shell vacancy only) to better than 5ppm is problematic in most cases.

Systematic measurements of all elements using up to date experimental techniques are in preparation [75]. But, the problem of the large natural line width and the satellite structure of the fluorescence X-rays could be overcome by using the narrow transitions of light exotic atoms and hydrogen-like electronic atoms.

7.1 Exotic atoms

The transition energies of completely stripped exotic atoms now are able to serve as a calibration standard for X-ray energies. For count rate reasons, pionic atoms are the most promising ones. As an example, the π^{14}N(5g-4f) transition has been used to obtain a value for the Sc Kα_1 transition energy which is a factor 6 more accurate than the value given in the published tables [29] (Table 1). The energy of the Ti Kα transition has been redetermined by the same method using the π^{20}Ne(6h-5g) transition [76]. A precise determination of the positions of diagram lines requires always a detailed study of the line shape [26,31,77].

7.2 ECR source

Transition energies and widths of hydrogen-like electronic systems can be calculated with the methods of QED to an accuracy of better than 1ppm. Because only radiative transitions occur, the line widths are of the order of 10 to 40 meV in the range from phosphorus to argon [43]. Such transitions would be much better suited to calibrate energies and to study the response functions of crystal spectrometers.

Low Z electronic atoms with few electrons can be produced with high intensity in Electron-Cyclotron-Resonance (ECR) devices as used as sources for atomic beams. It is proposed to build up such a device in using the cyclotron trap mirror field [73]. Then it will be possible to measure fluorescence X-rays and few electron systems with a crystal spectrometer in a fixed experimental set-up. A small Doppler broadening of a few 100 meV is expected from the Maxwellian velocity distribution inside the ECR source. For hydrogen-like electronic atoms, energy measurements on the sub ppm level for the 2p-1s diagram lines will become feasible which can be related to transitions from exotic atoms. The variety of transitions yields a dense net of transitions to be used as calibration standards.

Further applications of such a set-up would be the measurement of helium-like or few electron atoms in order to study various theoretical approaches of the electron-electron interaction [78], strong interaction effects in pionic atoms, or nuclear size effects in muonic atoms. In a first step, such an apparatus will be used to measure accurately the response function of the crystal spectrometer for the determination of the strong interaction broadening in pionic hydrogen [73].

8 Summary and outlook

A series of precision experiments is being performed of the characteristic X-radiation from exotic atoms. Main goals of the experiments are the determination of the hadronic level shifts and broadenings of the atomic 1s and 2p states in hydrogen isotopes, a new value for the mass of the charged pion, and the pion-nucleon scattering length from pionic hydrogen. The accurate knowledge of values for the pure electromagnetic part of the atomic energy levels is mandatory for the interpretation of those measurements.

Results from the experiments with antiprotons at LEAR are:

- The 2^3P_0 hyperfine state was resolved from the antiprotonic hydrogen Lα transition. The results for the strong interaction shift and broadening of the 2p hyperfine strongly support the prediction for the real part of the antinucleon-nucleon potential derived in the framework of the meson exchange model from the nucleon-nucleon interaction [47].
- The 2p-level strong-interaction effects in antiprotonic deuterium were observed by measuring the Lα transition being in reasonable agreement with the prediction of the multiple scattering approach [52].
- The line shape of the Lα transition in antiprotonic deuterium discards an earlier calculation of the electromagnetic hyperfine splitting in favor of a recent one [40,41,44].

The studies with pionic and muonic atoms at PSI yielded:

- The ambiguity of 15ppm for the mass of the charged pion from a previous high resolution experiment could be removed. Taking the weighted average of the results of [60] and [26], the presently reached accuracy for the pion mass is already less than 3ppm.
- The best test up to now of the Klein-Gordon equation to $4{\cdot}10^{-3}$ has been achieved from the πN(5g-4f) transitions [26].
- The Coulomb explosion in diatomic symmetric molecules has been directly observed from the line broadening of πN and the μO 5-4 transitions [63].
- The energies of fluorescence X-rays have been redetermined using transitions from hydrogen-like pionic atoms as calibration lines [76].

At PSI, in the near future,

- a high precision experiment of the charged pion mass to 1ppm will be performed by calibrating the πN(-4) transition energy with the μO(5-4) transition [27,63].

- The determination of the pion-nucleon scattering length and the pion-nucleon coupling constant to 1% has been started [73,74].
- For that, calibration measurements will be necessary using an ECR source implemented into the cyclotron trap which allows in addition the investigation of few electron systems [78].

Acknowledgements I am very grateful to the organizers of the workshop on "Frontier tests of QED and physics of the vacuum", 1998, for the generous support which enabled me to participate in that meeting at Sandansky, Bulgaria.

References

[1] G. Backenstoss, *Ann. Rev. Nucl. Sci* **20** (1970) 467
[2] *Proc. of The First Course on Exotic Atoms*, Erice, Italy, 1977
[3] *Proc. of the 2nd Workshop on Physics at LEAR* (U. Gastaldi and R. Klapisch, eds.), Erice, Italy, May 9-16, 1982, Plenum Publishing Corporation, New York 1984
[4] *Proc. of the Fifth Course of the International School of Physics of Exotic Atoms* (L. M. Simons, D. Horváth, and G. Torelli, eds.), May 14-20, 1989, Erice, Italy, Plenum Press, New York 1990
[5] F. Kottman, *QED tests with muonic atoms*, contribution to this workshop
[6] E. Borie and G. A. Rinker, *Rev. Mod. Phys.* **54** (1982) 67
[7] *PBAR: A Code for calculating the electromagnetic Contribution to the Energy Levels of Antiprotonic Atoms*, E. Borie and B. Jödicke, Comput. Phys. vol. **2**, no. 6 (1988) 61
[8] R. Bacher et al., *Phys. Rev.* **A 38** (1988) 4395
[9] R. Bacher et al., *Phys. Rev.* **A 39** (1989) 1610
[10] P. Vogel, P. K. Haff, V. Akylas, and A. Winther, *Nucl. Phys.* **A 254** (1975) 445
[11] J. S. Cohen and N. T. Padial, *Phys. Rev.* **A 41** (1990) 3460
[12] T. B. Day, G. A. Snow, and J. Sucher, *Phys. Rev. Lett.* **3** (1959) 61; T. B. Day, G. A. Snow, and J. Sucher, *Phys. Rev.* **118** (1960) 864
[13] E. Borie and M. Leon, *Phys. Rev.* **A 21** (1980) 1460
[14] K. Heitlinger et al., *Z. Phys.* **A 342** (1992) 359
[15] L. M. Simons, *Physica scripta* **T22** (1988) 90
[16] M. Schneider et al., *Z. Phys.* **A 338** (1991) 217
[17] L. M. Simons, *Hyperfine Interactions* **81** (1993) 253
[18] W. H. Zachariasen, *Theory of X-ray Diffraction in Crystals*, J. Wiley and Sons Inc., New York, 1947

[19] A. E. Sandström, *Handbuch der Physik*, **Band XXX**, Springer-Verlag, Berlin 1952
[20] S. Brennan and P. L. Cowan, *Rev. Sci. Instr.* **63** (1992) 850
[21] C. T. Chantler, *J. Phys. Chem. Ref. Data* vol. **24** (1995) no.1, 71
[22] H. H. Johann, *Z. Phys.* **69** (1931) 185
[23] J. Eggs and K. Ulmer, *Z. angew. Phys.*, **20. Band**, Heft 2 (1965) 118
[24] G. Fiorucci et al., Nucl. *Instr. Meth.* **A 292** (1990) 141
[25] D. Sigg, *Nucl. Instr. Meth.* **A 345** (1994) 197
[26] S. Lenz et al., *Phys. Lett.* **B 416** (1998) 50
[27] D. F. Anagnostopoulos et al., *PSI experiment R-97.02*, 1997
[28] R. Deslattes and T. Mooney, priv. comm.
[29] J. A. Bearden, *Rev. of Mod. Physics* **39** (1967) 78
[30] M. O. Krause and J. H. Oliver, *J. Phys. Chem. Ref. Data* **8** (1979) 329
[31] M. Deutsch et al., *Phys. Rev.* **A 51** (1995) 283
[32] S. Deser, L. Goldberger, K. Kaufmann, and W. Thirring, *Phys. Rev.* **96** (1954) 774
[33] T. L. Trueman, *Nucl. Phys.* **26** (1961) 57
[34] J. Carbonell, G. Ihle, and J. M. Richard, *Z. Phys.* **A 334** (1989) 329
[35] C. J. Batty, *Rep. Prog. Phys.* **52** (1989) 1165
[36] J. Carbonell, J.-M. Richard, and S. Wycech, *Z. Phys.* **A 343** (1992) 325
[37] D. Gotta, *Proc. of The 2nd Biennial Conf. on Low Energy Antiproton Physics (LEAP'92)* (C. Guaraldo, F. Iazzi, and A. Zenoni, eds.), Courmayeur, Italy, September 14-18, 1992, *Nucl. Phys.* **A 558** (1993) 645c
[38] D. Gotta, *Proc. of The 3rd Biennial Conf. on Low Energy Antiproton Physics (LEAP'94)* (G. Kernel, P. Krizan, and M. Mikuz, eds.), Bled, Slovenia, September 12-17, 1994, World Scientific, Singapur 1995, p. 525
[39] D. Anagnostopoulos et al., *LEAR experiment PS207*, proposal CERN/PSCC/90-9/P124 (1990)
[40] S. Barmo, H. Pilkuhn, and H. G. Schlaile, *Z. Phys.* **A 301** (1981) 283; H. Pilkuhn, priv. comm. (corrections)
[41] S. Boucard and P. Indelicato, priv. comm.
[42] P. Indelicato, priv. comm.
[43] H. A. Bethe, E. E. Salpeter, *Handbuch der Physik*, **Band XXXV**, Springer-Verlag, Berlin 1957
[44] E. Borie, [3], p. 561
[45] T. E. O. Ericson and J. Hüfner, *Nucl. Phys.* **B 47** (1972) 205
[46] J. J. Friar and G. L. Payne, *Phys. Rev.* **C 55** (1997) 2764
[47] D. F. Anagnostopoulos et al., *Proc. of The 4th Biennial Conf. on Low Energy Antiproton Physics (LEAP 96)* (H. Koch, M. Kunze, and K. Peters, eds.), Dinkelsbühl, Germany, August 27-31, 1996, *Nucl. Phys.* **B (Proc. Suppl.) 56 A** (1997) 84

[48] W. W. Buck, C. B. Dover, and J. M. Richard, *Ann. of Phys. (NY)* **121** (1979) 47
[49] C. B. Dover and J. M. Richard, *Phys. Rev.* **C 21** (1980) 1466
[50] C. W. E. van Eijk et al., *Nucl. Phys.* **A 486** (1988) 604
[51] D. Gotta et al., in preparation
[52] D. Anagnostopoulos et al., *Proc. of The 3rd International Conference on Nucleon-Antinucleon Physics (NAN'95)*, September 11-16, 1995, ITEP, Moskau, Russia, *Phys. of Atomic Nuclei (Yadernaya Fizika)* vol. **59**, no.9 (1996) 1503
[53] S. Wycech, A. M. Green, and J. A. Niskanen, *Phys. Lett.* **152 B** (1985) 308
[54] S. L. Glashow, *Phys. Lett.* **187 B** (1987) 367
[55] H. Harari and Y. Nir, *Nucl. Phys.* **B 292** (1987) 251
[56] L. Willmann et al., *Phys. Rev. Lett.*, to be published
[57] P. Herczeg and R. N. Mohapatra, *Phys. Rev. Lett.* **69** (1992) 2475
[58] D. Sigg et al., *Nucl. Phys.* **A 609** (1996) 310
[59] B. Jeckelmann et al., *Nucl. Phys.* **A 457** (1986) 709
[60] B. Jeckelmann et al., *Phys. Lett.* **B 335** (1994) 326
[61] K. Assamagan et al., *Phys. Rev.* **D 53** (1996) 6065
[62] V. R. Akylas and P. Vogel, *Comp. Phy. Comm.* **15** (1978) 291
[63] Th. Siems, *thesis*, University of Cologne, 1997; Th. Siems et al., in preparation
[64] L. Delker et al., *Phys. Rev. Lett.* **42** (1979) 89
[65] P. Ehrhart et al., *Z. Phys.* **A 311** (1983) 259
[66] S. Chelkowski and A. D. Bandrauk, *J. Phys.* **B 28** (1995) 723
[67] V. Bernard, N. Kaiser, and U.-G. Meissner, *Phys. Rev.* **C 52** (1995) 2185
[68] U.-G. Meissner et al., hep-ph/9711361
[69] D. Chatellard et al., *Nucl. Phys.* **A 625** (1997) 855
[70] E. C. Aschenauer et al., *Phys. Rev.* **A 51** (1995) 1965
[71] A. Badertscher et al., *Phys. Lett.* **B 392** (1997) 278
[72] L. Bracci and G. Fiorentini, *Nuovo Cim.* **43 A** (1978) 9
[73] G. C. Oades et al., *PSI proposal R-98.01*, 1998
[74] D. F. Anagnostopoulos et al., *Ann. rep. IKP 1997*, Forschungszentrum Jülich, Jül-**3505**, 1998, p.86; D. F. Anagnostopoulos et al., submitted to *Phys. Rev. Lett.* **C**
[75] R. Deslattes, P. Indelicato et al., in preparation
[76] D. F. Anagnostopoulos et al., in preparation
[77] D. F. Anagnostopoulos, M. Deutsch, D. Gotta, and R. Sharon, *Kα and Kβ X-ray emission of scandium*, in preparation
[78] P. Indelicato, *Short note on the status of the physics of one and two electron systems*, unpublished, 1998